www.czasopisma.pan.pl PAN POLSKA AKADEMIA NAUK www.journals.pan.pl

Arch. Metall. Mater. **64** (2019), 2, 715-719

DOI: 10.24425/amm.2019.127603

K. GLOWKA*, M. ZUBKO*,**#, P. ŚWIEC*, K. PRUSIK*, G. DERCZ*, E. MATYJA*, D. STRÓŻ*

MICROSTRUCTURE OF MULTI-COMPONENT $Ni_{35}Ti_{35}Ta_{10}Co_{10}Cu_{10}$ ALLOY

A new NiTi-based multi-component $Ni_{35}Ti_{35}Ta_{10}Co_{10}Cu_{10}$ (at.%) alloy was obtained by vacuum arc melting. The microstructure of the alloy has been studied using scanning and transmission electron microscopy, backscatter electron diffraction and X-ray diffraction techniques. The performed measurements showed presence of two cubic and one tetragonal phases. Energy dispersive X-ray spectroscopy analysis confirmed that all the observed phases contained all five principal elements.

Keywords: High Entropy Alloys, Multi-component alloys, electron microscopy, microstructure

1. Introduction

High Entropy Alloys (HEAs) are a group of multi-component materials that gain attention of many research groups in recent years. Yeh [1], one of the creators of HEAs, provided two definitions: HEAs are alloys composed of at least five principal elements where concentration of each is between 5÷35 at. %. The second definition is based on configurational entropy, in which HEAs are defined as alloys having configurational entropy at random state (Eq. (1)) greater than or equal to $1.5 \cdot R$ (where: R is a gas constant), no matter whether they are single phase or multiphase at room temperature [1]:

$$\Delta S_{conf} = -R\sum_{i=1}^{N} x_i \ln x_i \tag{1}$$

where x_i is atomic fraction of i^{th} element. In traditional alloys, phase composition can be controlled by Gibbs free energy (G). In the case of a phase formation, the Gibbs free energy can be related to enthalpy (H) or entropy (S) [2]. In high entropy alloys additionally to these parameters there are proposed also supplementary parameters correlated with a phase formation. These are: atomic size mismatch δ calculated from $\delta = 100\%\sqrt{\sum_{i=1}^{n} c_i\left(1-\frac{r_i}{\bar{r}}\right)^2}$, where c_i and r_i denote the atomic fraction and atomic radius of the i^{th} element respectively, mixing enthalpy $-\Delta H_{mix}$ calculated from $\Delta H_{mix} = \sum_{i=1, i\neq j}^{n} 4\Delta H_{mix}^{AB} c_i c_j$, where c_i, c_j are atomic fraction of i^{th}, j^{th} element and ΔH_{mix}^{AB} is mixing enthalpy of binary liquid AB alloys, electronegativity difference $\Delta\chi$ calculated from $\Delta\chi = \sqrt{\sum_{i=1}^{n} c_i\left(\chi_i - \bar{\chi}\right)^2}$, $\bar{\chi} = c_i\chi_i$ where χ_i is Pauling electronegativity for the i^{th} component, valence electron parameter VEC calculated from $VEC = \sum_{i=1}^{n} c_i\left(VEC\right)_i$, where $(VEC)_i$ is valence electron concentration of i^{th} element – described below. The atomic size is a crucial parameter in forming of solid solutions which can be clearly seen in the classic Hume-Rothery rules. [3]. Basing on the atomic radii of elements it is possible to calculate the atomic size mismatch (δ) which in case of HEAs should be in 0÷5% range [4]. Enthalpy is the next parameter which can be used to classify the HEAs and is useful to characterize chemical compatibility from many principal components. In the case of HEAs, this parameter is defined as mixing enthalpy (ΔH_{mix}) and should be in –5÷–15 kJ/mol range [4,5]. The electronegativity difference parameter ($\Delta\chi$) is correlated with elemental segregation in alloys [6] and the formation of topologically close-packed (TCP) phases [7]. The valence electron parameter (VEC) is a parameter which can suggest formation of *bcc* or *fcc* type of structure of solid solutions [8]. It was shown that the $\Delta\chi$ and VEC parameters are not strongly correlated with phase selection between solid solutions, intermetallic and amorphous phase. When ΔS_{mix} parameter is higher, in effect solid solutions form.

The increased interests in high entropy alloys are due to their interesting properties especially mechanical properties. Thanks to these properties HEAs can have many potential applications e.g. engine materials [9], nuclear materials [10], refractory materials [11]. The high entropy $Co_{1.5}CrFeNi_{1.5}Ti_{0.5}$ (at.%) alloy

* UNIVERSITY OF SILESIA, INSITUTE OF MATERIALS SCIENCE, 75 PUŁKU PIECHOTY 1A STR., 41-500 CHORZÓW, POLAND
** UNIVERSITY OF HRADEC KRÁLOVÉ, DEPARTMENT OF PHYSICS, HRADEC KRÁLOVÉ, CZECH REPUBLIC
# Corresponding author: maciej.zubko@us.edu.pl

obtained by casting methods found applications in daily life i.e. it is used for fabrication of bearings due to its increased wear resistance properties [9].

Recently, studies on high entropy alloys are focused on obtaining materials exhibiting shape memory effect. This group of HEA can be called High Entropy Shape Memory Alloys – HESMAs [10]. They can be also defined as High-Temperature Shape Memory Alloys (HTSMAs) because their characteristic temperatures of martensitic transformation are above room temperature [11]. These characteristic temperatures of martensitic transformation (MT) can be controlled by the chemical composition of the alloys. The composition obtained by G. Firstov et al. $Ti_{16.667}Zr_{16.667}Hf_{16.667}Co_{5/10}Ni_{20/25}Cu_{16.667/25}$ was proposed as high entropy shape memory alloys and high-temperature shape memory alloys [10-11].

The area of multi-component alloys is relatively young and there is still lot of gaps in the knowledge regarding the phase composition and microstructure of those alloys. Thus, the idea of the work was to produce and characterise a new multi-component alloy composed of 5 principal elements and that would possibly show shape memory effects additionally to the typical properties of HEAs. The elements such as Co, Cu and Ta were chosen and added to NiTi alloy because the NiTi with the additions of these elements show shape memory effects.

2. Materials and methods

$Ni_{35}Ti_{35}Ta_{10}Co_{10}Cu_{10}$ alloy was obtained by vacuum arc melting in Ar protective gas atmosphere (pressure of 1.2 bar). During fabrication the material was remelted five times in order to obtain better homogeneity. During the arc melting process the material button was completely melted and commingled for approximately 1 minute for each cycle. The alloy was prepared from commercially available: nickel, titanium and copper pellets (a purity 99.999%), tantalum plates (a purity 99.999%) and cobalt lump (a purity 99.999%). The parameters describing the multi-component alloys (mentioned earlier: atomic size mismatch – δ, mixing enthalpy – ΔH_{mix}, mixing entropy – ΔS_{mix}, electronegativity differences – $\Delta\chi$, valence electron parameter – *VEC*) were calculated for the studied alloy (see Table 1) and compared with literature compositions of Firstov $Ti_{16.667}Zr_{16.667}Hf_{16.667}Co_{0/16.667}Ni_{16.667/25}Cu_{16.667/25}$ HEA exhibiting shape memory effect [12-13].

The microstructure images in the secondary electrons contrast were taken using the JEOL JSM-6480 scanning electron microscope (SEM working with the accelerating voltage of 20 kV) equipped with the electron backscattered diffraction (EBSD) system from HKL and Nordlys II detector and the Energy Dispersive X-ray Spectroscopy (EDS) detector form IXRF. The microstructure was also studied using JEOL JEM-3010 high-resolution transmission electron microscope (TEM) with 300 kV acceleration voltage, equipped with a Gatan $2k \times 2k$ Orius™ 833 SC200D CCD camera. Thin foil samples for TEM measurements were cut into pieces with diameter $d = 3$ mm and ~100 μm thickness. Next, the samples were grinded on both sides and Ar – ion polished on Gatan Precision Ion Polishing System (PIPS). The recorded selected area electron diffraction (SAED) patterns were indexed using the ElDyf computer software. Phase composition was studied basing on X-ray powder diffraction measurements performed on a Panalytical Empyrean diffractometer with Cu anode ($Cu_{K\alpha} - \lambda = 1.54056$ Å) working at an electric current of 30 mA and voltage of 40 kV and equipped with a PIXcell^{3D} detector. The phase analysis was performed using reference standards from the International Centre for Diffraction Data (ICDD) PDF-4 database.

3. Results

3.1. Phase analysis using X-ray Diffraction

X-ray phase analysis was performed in the angular range of $2\theta = 10 \div 110°$. Diffraction pattern for as – received sample is shown in Fig. 1.

Using the PDF4+ ICDD (International Centre for Diffraction Data) database the presence of three phases was revealed. The first (dominant) phase was identified as cubic phase with the space group $Pm\bar{3}m$ and lattice parameter $a_0 = 3.0130$ Å similar to TiNi (PDF ICDD 04-017-2083). The second phase was identified as tetragonal phase with the space group I4/mmm similar to (CuNi)Ti (PDF ICDD 01-079-3634) and lattice parameters $a_0 = 3.1200$ Å and $c_0 = 7.9650$ Å and the last phase is also cubic with the space group $Fd\bar{3}m$ and lattice parameter $a_0 = 11.330$ Å similar toTi_2Ni (PDF ICDD 04-003-6277). The diffraction pattern of the as – received material shows the strongest diffraction peak for $2\theta = 42°$, which represents {110} planes corresponding to the phase similar to TiNi. All main parameters of the phases are summarized in Table 2.

TABLE 1

Calculations of valence electron concentration (*VEC*), electronegativity differences ($\Delta\chi$), atomic size mismatch (δ), enthalpy of mixing (ΔH_{mix}) and entropy of mixing (ΔS_{mix}) for present studies and G. Firstov compositions

Alloys	*VEC* [8]	$\Delta\chi$ [6]	δ [4]	ΔH_{mix} [kJ/mol] [4-5]	ΔS_{mix} [J/mol·K] [Eq. (1)]	References
$Ni_{35}Ti_{35}Ta_{10}Co_{10}Cu_{10}$	7.40	0.19	7.54	–26.33	–11.90	This study
$Ti_{16.667}Zr_{16.667}Hf_{16.667}Ni_{25}Cu_{25}$	7.25	0.27	10.66	–28.17	–13.20	[13]
$Ti_{16.667}Zr_{16.667}Hf_{16.667}Co_{16.667}Ni_{16.667}Cu_{16.667}$	7.00	0.26	10.79	–29.89	–12.40	[13]

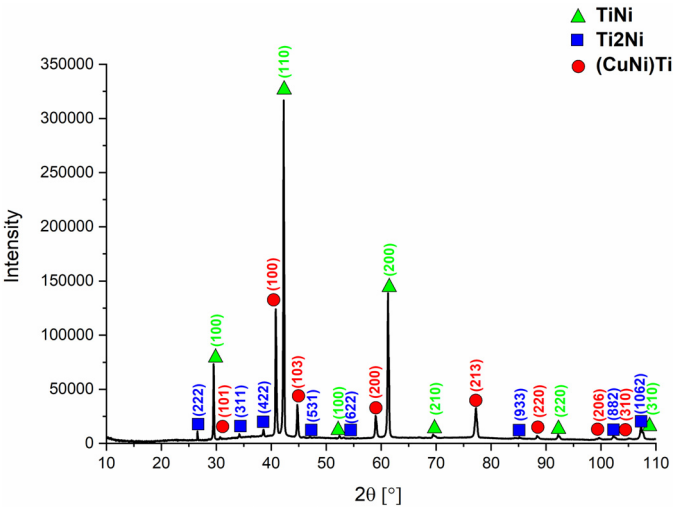

Fig. 1. X-ray diffraction pattern for as – received material

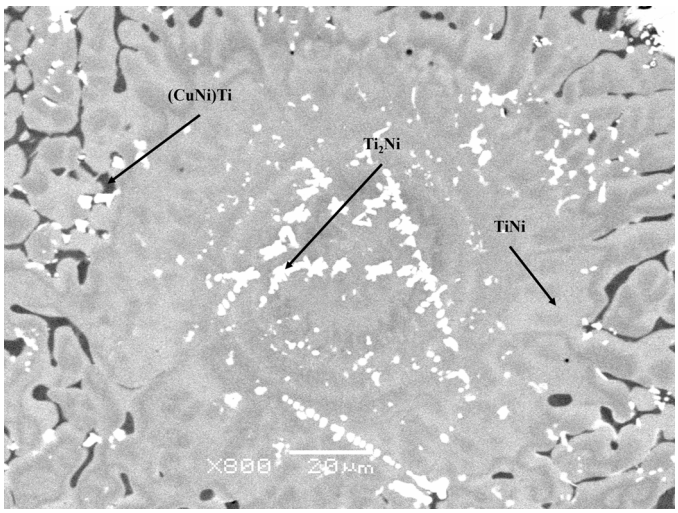

Fig. 2. SEM microstructure images with assigned phases for as – received material

TABLE 2

Main parameters of phases from ICDD for as – received material

Phase	TiNi	(CuNi)Ti	Ti_2Ni
Crystal structure	Cubic	Tetragonal	Cubic
Space group	$Pm\bar{3}m$	I4/mmm	$Fd\bar{3}m$
Lattice parameters from ICDD [Å]	$a_0 = 3.0130$	$a_0 = 3.1200$ $c_0 = 7.9650$	$a_0 = 11.3330$
ICDD	04-017-2083	01-079-3634	04-003-6277

3.2. Microstructure

In order to perform microstructure analysis Scanning Electron Microscopy (SEM) measurements in secondary electrons imaging was performed. The recorded images clearly show three different contrast areas corresponding to a different chemical composition of each phase (Fig. 2).

Microstructure analysis confirmed the presence of three phases what is in agreement with the results of X-ray diffraction measurements analysis.

EBSD method allowed resolving the observed phases on SEM images. The obtained Kikuchi diffraction patterns (Fig. 3) were indexed basing of the phases determined by X-ray diffraction measurements and were assigned to different contrast regions in the observed microstructure image (Fig. 2). The EBSD method confirmed presence of phases similar to (CuNi)Ti, TiNi and T_2Ni phases in studied alloy.

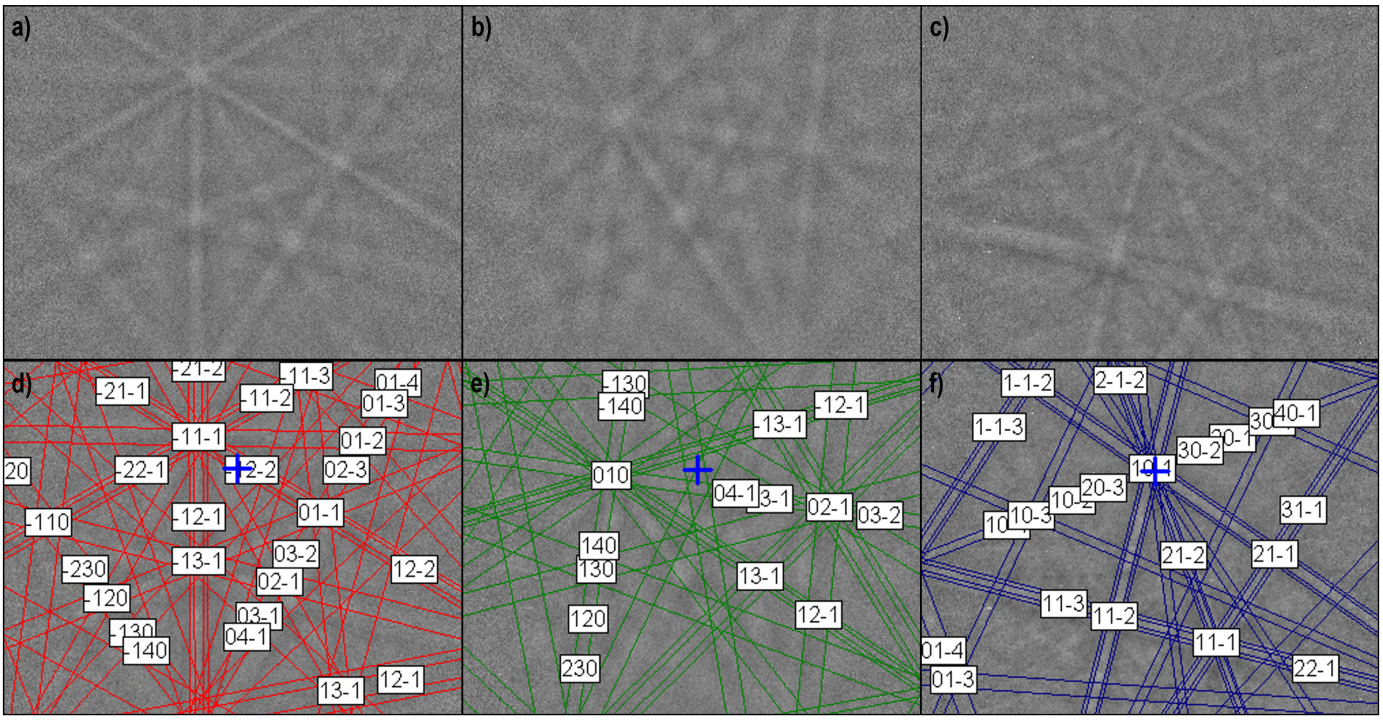

Fig. 3. Kikuchi lines and indexed patterns for (a-d) (CuNi)Ti, (b-e) TiNi, (c-f) Ti_2Ni phases

Using Energy Dispersive X-Ray Spectroscopy method an average chemical composition for all the phases was determined. It was found that all the observed phases contained all five principal chemical elements but there were some differences in content depending on the phase. For the as – received alloy the EDS measurements showed that for the phase with the structure of TiNi phase the average chemical composition is close to the nominal one. The phase similar to (CuNi)Ti phase is enriched in Ni, Ti, Cu elements and depleted in Co and Ta. The phase similar to Ti_2Ni phase is enriched in Ni, Ti, Ta and depleted in Co and Cu. Based on the recorded SEM images and using ImageJ software for image analysis percentage surface fraction of the phases was calculated. The analysis was performed for 4 fields of view with a total area of ~0.56 mm^2. The calculations confirmed the observations from X-ray diffraction measurements – the highest volume fraction was taken by the phase similar to TiNi phase (Table 3).

For detailed microstructure analysis transmission electron microscopy measurements were performed. Bright field images and corresponding selected area electron diffraction patterns are shown in Fig. 4.

They confirmed the presence of phases similar to (CuNi)Ti, TiNi and Ti_2Ni phases.

TABLE 3

Average chemical composition and percentage surface fraction

Phase	Elements and average at.%					Percentage surface fraction [%]
TiNi	Ni	Ti	Co	Cu	Ta	83.1
	33.2	34.9	9.9	8.8	11.4	
(CuNi)Ti	Ni	Ti	Co	Cu	Ta	12.2
	36.1	27.7	3.9	19.0	8.6	
Ti_2Ni	Ni	Ti	Co	Cu	Ta	4.7
	25.3	42.0	7.3	5.4	19.7	

4. Conclusion

The new NiTi-based multi-component $Ni_{35}Ti_{35}Ta_{10}Co_{10}Cu_{10}$ (at.%) alloy was obtained. Three phases were observed in the alloy, they were similar to: B2 phase of TiNi, (CuNi)Ti, and Ti_2Ni phases, which was confirmed by all presented methods. The performed EDS analysis showed that all the observed phases contained all five principal elements. The dominant phase of the TiNi structure has chemical composition congruous with the nominal one for the fabricated alloy. The two other phases are mostly enriched in Cu, Ni, Ti (for (CuNi)Ti phase), and in Ni, Ti, Ta (for Ti_2Ni phase). Unfortunately, the alloy did not show shape memory effects.

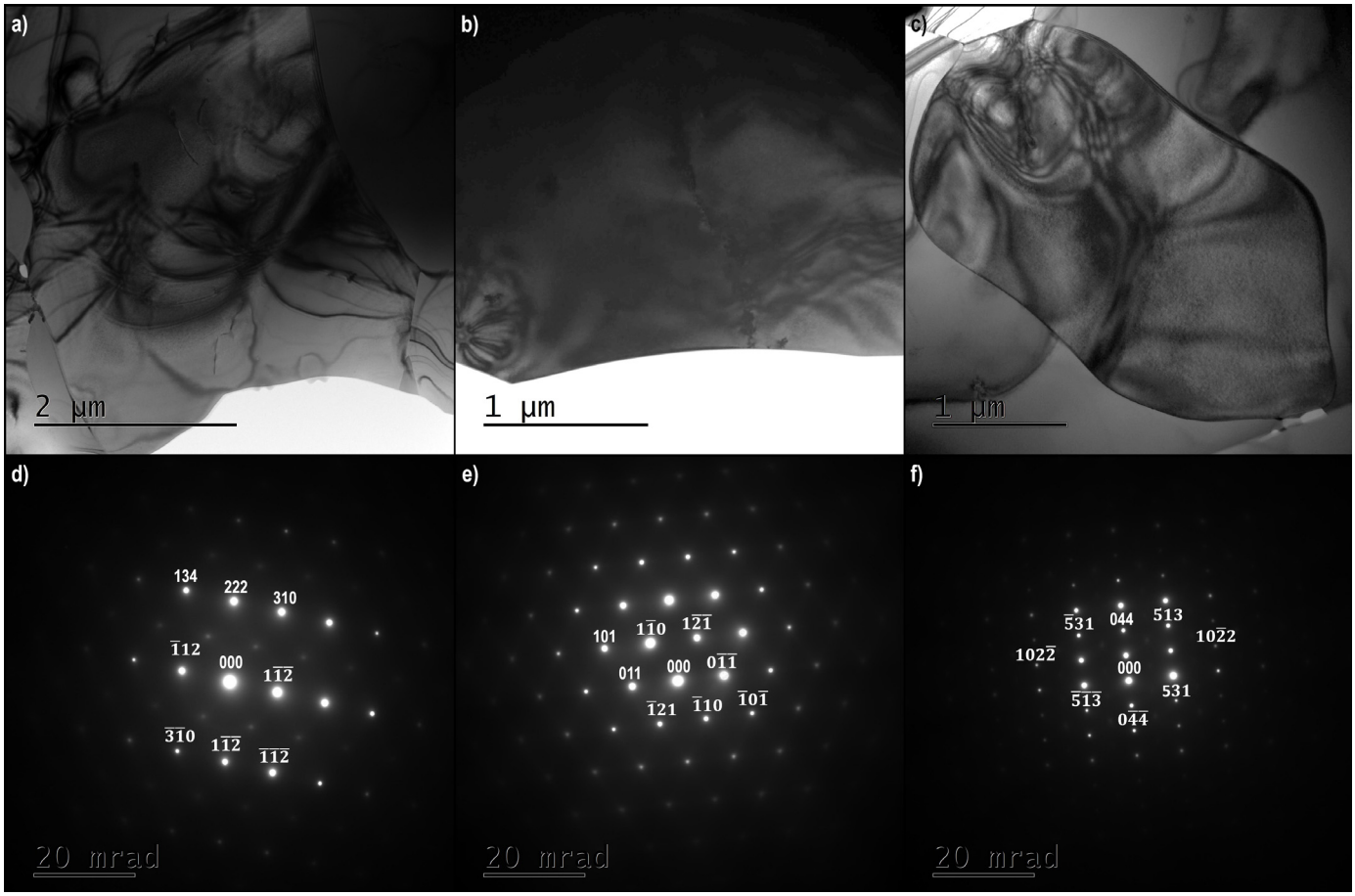

Fig. 4. TEM bright field and indexed corresponding selected area electron diffraction patterns for (a-d) (CuNi)Ti, (b-e) TiNi, (c-f) Ti_2Ni phases

REFERENCES

[1] B.E. MacDonald, Z. Fu, B. Zheng, W. Chen, Y. Lin, F. Chen, L. Zhang, J. Ivanisenko, Y. Zhou, H. Hahn, E.J. Lavernia, JOM **69** (10), 2024-2031 (2017), DOI: https://doi.org/10.1007/s11837-017-2484-6

[2] S. Guo, Mater. Sci. Technol. **31** (10) 1223-1230 (2015). DOI: https://doi.org/10.1179/1743284715Y.0000000018

[3] R.W. Cahn, P. Hassen, Physical metallurgy 1. 4th Edition, North Holland, Amsterdam (1996).

[4] Y. Zhang, Y.J. Zhou, J.P. Lin, G.L. Chen, P.K. Liaw, Adv. Eng. Mater. **10** (6), 534-538 (2008), DOI: https://doi.org/10.1002/adem.200700240

[5] A. Takeuchi, A. Inoue, Mater. Trans. **41** (11), 1372-1378 (2000), DOI: https://doi.org/10.2320/matertrans1989.41.1372

[6] Z.S. Nong, J.C. Zhu, Y. Cao, X.W. Yang, Z.H. Lai, Y. Liu, Mater. Sci. Technol. **30** (3), 363-369 (2014), DOI: https://doi.org/10.1179/1743284713Y.0000000368

[7] Y. Dong, Y.P. Lu, L. Jiang, T.M. Wang, T.J. Li, Intermetallics **52** (9), 105-109 (2014), DOI: https://doi.org/10.1016/j.intermet.2014.04.001

[8] S. Guo, C. Ng, J. Lu, C.T. Liu, J. Appl. Phys. **109** (10), 1-5 (2011), DOI: https://doi.org/10.1063/1.3587228

[9] B.S. Murty, J.W. Yeh, S. Ranganathan, High Entropy Alloys, Butterworth-Heinemann, London (2014).

[10] T. Yang, S. Xia, S. Liu, C. Wang, S. Liu,Y. Fang, Y. Wang, Sci Rep – UK **6** (4), 1-8, (2016). DOI: https://doi.org/10.1038/srep32146

[11] O.N. Senkov, J.M. Scott, S.V. Senkova, F. Meisenkothen, D.B. Miracle, C.F. Woodward, J. Mater. Sci. **47** (9), 4062-4074, (2012). DOI: https://doi.org/10.1007/s10853-012-6260-2

[12] G.S. Firstov, T.A. Kosorukova,Y.N. Koval, V.V. Odnosum, Mater. Today Proc. **2**, 499-504 (2015). DOI: https://doi.org/10.1016/j.matpr.2015.07.335

[13] G.S. Firstov, T.A. Kosorukova, Y.N. Koval, P.A. Verhovlyuk, Shape Mem. Superelasticity **1** (4), 400-407 (2015), DOI: https://doi.org/10.1007/s40830-015-0039-7